

Influences of the heating and plasma density on impurity production and transport during the ramp-down phase of JET ILW discharge

I. Ivanova-Stanik¹, R. Zagórski², A. Chomiczewska¹, P.Lomas³,
I. Voitsekhovitch³, D. R. Ferreira⁴, C. Sozzi⁵, E. Joffrin⁶, E.
Lerche⁷ and JET Contributors ‡

EUROfusion Consortium, JET, Culham Science Centre, Abingdon, OX14 3DB, UK

¹Institute of Plasma Physics and Laser Microfusion, Hery 23, 01-497 Warsaw, Poland

²National Centre for Nuclear Research (NCBJ), 05-400, Otwock, Poland

³CCFE, Culham Science Centre, Abingdon, Oxon, OX14 3DB, UK

⁴Instituto Superior Técnico (IST), University of Lisbon, Portugal

⁵Istituto di Fisica del Plasma -CNR, Milano, Italy

⁶CEA, IRFM, F-13108 Saint-Paul-lez-Durance, France

⁷LPP-ERM/KMS, Association EUROFUSION-Belgian State, TEC partner, Brussels, Belgium

E-mail: irena.ivanova-stanik@ifpilm.pl

November 2020

Abstract. The aim of this paper, is to study the influence of the plasma heating and plasma density on impurity production and transport during the plasma termination phase. We have analysed the ramp-down phase of a set of representative high current JET ILW discharges: # 92437 (disrupted) and # 92442 (soft landing) characterized with high plasma current $I_p = 3.5\text{MA}$. The analysis is performed for different time slots at the ramp-down phase, corresponding to different levels of the electron line density and auxiliary heating power. Since the deuterium gas fluxes are different, the influence of the separatrix density is also analysed. The main conclusion from simulations is the observation that for the same average electron density, a decrease of the separatrix density leads to an increase of the plasma temperature at the divertor plate leading to increased W production and consequently to larger W concentration and radiation in the core. When the central electron temperature approaches the 2keV level, corresponding to the maximum of the W and Ni cooling rate, the radiation in the plasma center is enhanced. The Ni radiation is more important in the ramp-down phase.

Keywords: tokamak, JET discharges, ramp-down, integrated modelling

‡ See the author list of E. Joffrin et al. 2019 Nucl. Fusion 59 112021)

1. Introduction

One of the major problems in present tokamaks is the presence of disruptions. Disruptions occur due to loss of stability and/or confinement of tokamak plasmas [1]. Because of the fast time scale (several tens of milliseconds) on which the plasma thermal and electromagnetic energy are released, strong electromagnetic forces (several MN) and large thermal loads on the surrounding components can be induced. Understanding of disruptions plays an important role for design of the future fusion devices as they cause large thermal and mechanical loads on the machine structure. The magnitude of these arise from a combination of physics, structural and thermal engineering considerations and from inherent limits on the thermal energy handling capabilities of materials available for plasma-facing component surfaces.

JET with carbon (C) wall and divertor has operated previously with a low frequency of disruptions [2] (i.e. disruption rate) of 3.4% . The analysis of pure Ohmic and L-mode current-ramp-down phase of three JET hybrid pulses is shown in Ref. [3]. JET disruption rate has dramatically increased with the ITER-like wall (ILW, equipped with W divertor, and Be wall) [4]. JET discharges with the new ITER-like wall has changed the radiation distribution towards higher plasma core radiation. Switching off the power at termination, as was done with the JET-C, often result in a radiative collapse and a disruption.

The disruptivity in JET discharges with the new ILW can exceed 30%. Disruptions in a tokamak can cause dramatic damage to the device. The tolerable heat loads with the ILW are more restricted because of the potential for melting of the tungsten coated tiles at the target or beryllium PFCs in the main chamber. Disruptions are a critical issue for ITER. The new wall in JET is a unique test bed to study disruptions under ITER-like conditions. The material of the PFCs has significant impact on the disruption properties and related loads [5].

The understanding of the physics of the causes of disruptions remains an important subject of investigations in order to reduce disruptivity, particularly for the ITER-relevant high density and high current operation. The current ramp-down (RD) of a burning plasma is a challenging part of plasma operation in any fusion reactor and ramp-down simulations and modelling studies have acquired particular importance in a number of works published recently [6],[7]. The control of the ELM frequency is beneficial and can play an important role in preventing the contamination of the plasma by W in metallic wall devices [8, 9]. Strategies are being developed in present experiments to avoid W accumulation in stationary phases of H-mode discharges by ELM triggering to control the edge W density and by central RF heating to prevent core accumulation. On the other hand, the control of W transport can be more challenging during the confinement transient phases between L-mode and H-mode and in particular in the transition from stationary H-mode to L-mode. During this phase the pedestal as the input power is decreased. This can lead to reduced ELM frequencies and extended intermittent ELM-free phases causing uncontrolled increase of the edge W density and

peaking of the core density profile, which is favorable for W accumulation. The required ELM frequency to avoid W accumulation could be achieved at JET through adjustment of the gas fuelling level or/and by active ELM control with pellets or kicks (fast vertical plasma motion at an adjustable frequency) [10, 11].

Investigation of ramp-down scenario performed at JET ILW is presented in this work. We have analysed the ramp-down phase of a set of representative high current JET ILW discharges. As a first step we have analysed the experimental data for two discharges: # 92437 (disrupted) and # 92442 (soft landing) with high plasma current $I_p = 3.5\text{MA}$. Both shots are similar before the start of the termination of the discharge at 13.9s, but shot # 92437 develops a hollow temperature profile which runs away to disruption. The main question is whether there is a difference in impurity content or other critical plasma parameters before the start of termination or a difference in impurity source or transport during the termination phase.

Since the energy balance in tokamaks with a tungsten divertor depends strongly on the coupling between bulk and the SOL plasma, proper modelling requires joint treatment of both regions. Our approach is based on integrated numerical modelling of plasma parameters using the COREDIV code, which self-consistently solves the 1D radial transport equations of plasma and impurities in the core region and 2D multi-fluid transport in the SOL. The COREDIV code was successfully benchmarked against a number of JET discharges with tungsten divertor and beryllium wall (JET ILW) for nitrogen [12, 13] and neon [14] seeding, proving its capability of reproducing the main features of JET seeded discharges.

In particular, we have analysed the influence of the plasma heating and plasma density at the separatrix on impurity production and transport during the plasma termination phase. Since COREDIV assumes a slab geometry in the SOL, the objective of COREDIV studies is to explore the dependencies of impurities transport with power and density but not necessarily to reproduce the exact behaviour of the pulses.

2. Model

As this work is a follow-up of our previous simulations for JET ILW, the detailed description and parameters used can be found in Refs. [15, 14, 16] and only the main points of the model are reported here. In the core, the 1D radial transport equations for bulk ions, for each ionization state of impurity ions and for the electron and ion temperatures are solved. In the SOL, the 2D fluid equations are solved in the simplified slab geometry, neglecting in-out asymmetry of the problem. Therefore the simulation results for divertor parameters should be treated as averaged over two divertor legs. In practice, it means that they are more representative for the outer divertor parameters since the inner divertor in JET is usually detached.

COREDIV takes into account the plasma and seeded impurities recycling in the divertor as well as the sputtering processes at the target plates including W sputtering by deuterons, self-sputtering and sputtering due to seeded impurities. (For deuterium,

neon, nickel sputtering and tungsten self-sputtering the yields given in [17] are used). The recycling coefficient of the main ions is an external parameter which in COREDIV depends on the level of the electron density at the separatrix, n_{es} , given as an input [12].

The experimental in-out asymmetries, observed especially at high density-high radiation level, are not reproduced in COREDIV results due to the geometrical simplifications of the COREDIV model. Although the simulations refer to the inter-ELM phase of the discharges, since production as well as flushing out of W due to ELMs is not accounted for in the present model. It should be noted, that for the analysed shots in the ramp-down phase ELM-free periods is observed.

The model provides main plasma parameters (profile on the density, temperature, effective ion charge, impurity concentration, impurity and total radiation, power and temperature to the plate), from a number of inputs like the auxiliary heating power, the average volume electron density $\langle n_e \rangle^{VOL}$, the confinement enhancement factor H_{98} and the separatrix density n_{es} . For the COREDIV code, which self-consistently solves 1D radial transport equations for plasma and impurities in the core region and 2D multi-fluid transport in the SOL, the density at the separatrix is one of the most important parameters and has strong influence on the impurity radiation in the core. The coupling between core and edge regions is especially relevant in the case of the tungsten, where changes in the edge (with related changes in the W fluxes) may lead to significant changes in the radiated power level in the core, then, in turn, in the power entering the SOL. The separatrix electron density is an important interface parameter for core performance and divertor power exhaust.

In the experiment, the leading parameter determining n_{es} was found to be the neutral divertor pressure [18], which can be considered as an engineering parameter since it is determined mainly by the gas puff rate and the pumping speed. In ASDEX Upgrade, measurements of the upstream separatrix density for N seeded and unseeded H-modes reveal a strong correlation with the divertor neutral pressure. Under stationary conditions, the divertor pressure can be regarded as an engineering parameter being largely proportional to the gas puff rate. Therefore, we assume similar situation on JET ILW.

3. Experimental results

We have analysed the experimental data for two discharges: # 92437 (disrupted) and # 92442 (soft landing) characterized with high plasma current $I = 3.5\text{MA}$ and high toroidal magnetic field $B_T = 3\text{T}$. The time slice evolution of the main parameters: auxiliary power, gas puffing, total and core radiation, effective charge (Z_{EFF}), electron temperature at magnetic axis ($T_e(0)$), line average electron density (n_e^{LINE}) and plasma current (I_p) are shown in Fig.1 for shot # 92347 and Fig.2 for shot # 92442.

The experimental study of the W concentration in the JET ILW configuration is based on a deconvolution of signals from the SXR-cameras [19] with the approach

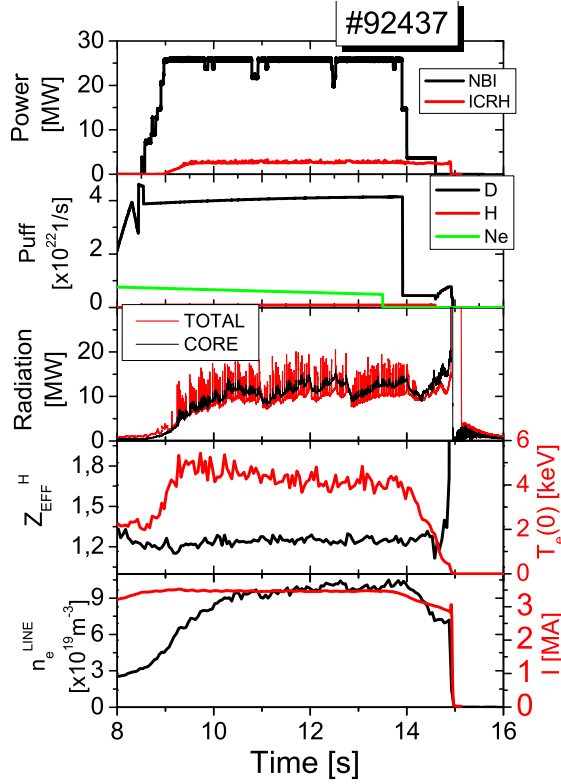


Figure 1. The time slices for shot #92437.

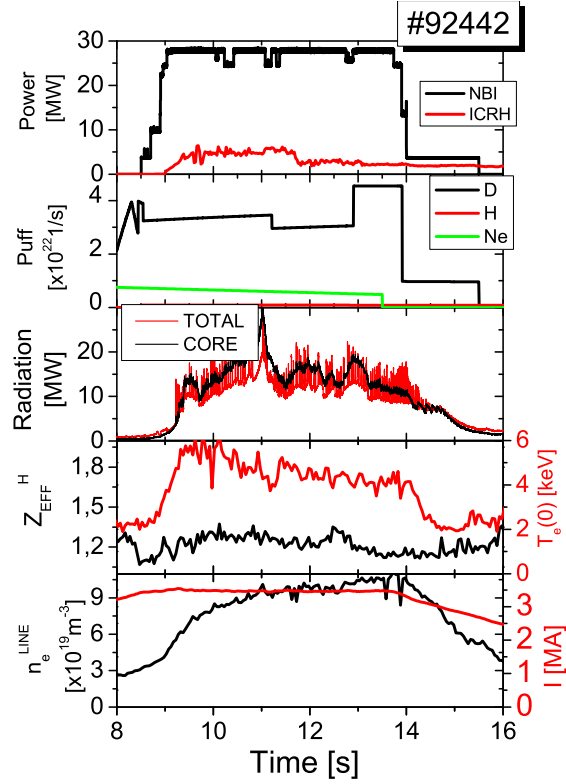


Figure 2. The time slices for shot #92442.

described in detail in Ref.[20, 21]. It was assumed that the main radiator in soft X-ray is W, while the radiation from other metallic impurities is negligible. In Fig.3a, we present time evolution of W concentration for both shots. As a first observation (see Fig.3a, the W concentration is similar for both shots at time $t = 13.9$ s for three position at the normalised radius (r/a): 0.0 (centre), and 0.45 before the start of ramp-down. After reduction of the D puff at $t = 13.9$ s to 4.4×10^{21} 1/s for #92437, which is about 2 times smaller compared to shot #92442 (see Fig.1 and Fig.2), the W concentration starts to increase. It can be seen that W concentration is higher at the time $t < 14.5$ s for the shot with lower D puff (#92437).

In Fig.3b, we show the Ni concentration (C_{Ni}) for both shots obtained from measurement of the VUV survey spectrometer (known as KT2 [22] diagnostic at JET) for position at the normalised radius 0.5-0.6. It can be seen that Ni behaves similarly to W. In the case of the disruptive shot (#92437), we observe an increase of the Ni density (concentration is not changed) from 13.9s to 14.25s which is connected to the decrease of the electron density see Fig.1 and for $t > 14.25$ s C_{Ni} starts to increase.

The comparison of the time evolution of the D_α and tungsten WI emission in divertor for both shots is presented in Fig.3c and Fig.3d, respectively. We observe small difference in ELMs in both shots of about 20% (see Fig.3c), which could have influence on the higher W and Ni concentration for #92437 (see Fig.3a and Fig.3b).

At the time when the ramp-down phase starts ($t > 13.9$ s), as the input power (NBI)

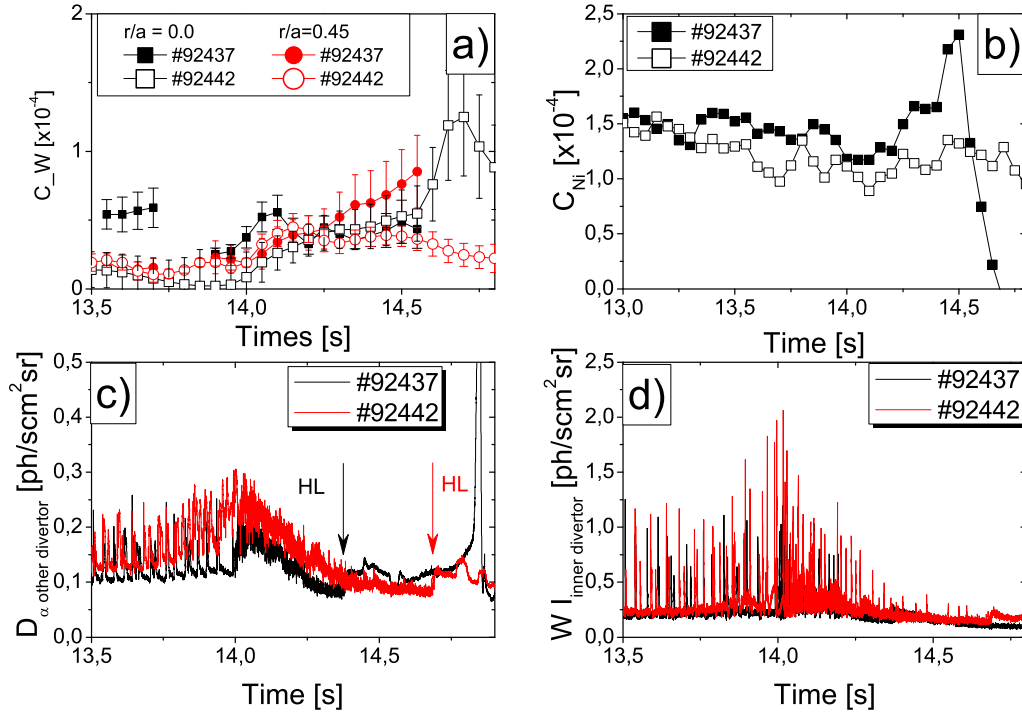


Figure 3. Time evolution for: W concentration based on soft X-ray for #92437 (full symbol) and #92442 (open symbol) for two different position at the normalized radius ($r/a = 0; 0.45$) (a), Ni concentration for #92437 (open symbol) and #92442 (full symbol) for position at the normalized radius ($r/a = 0.5 \div 0.6$) (b), emission of the D_{α} (c) and WI in inner divertor (d).

is decreased, for $t > 14.2\text{s}$ an extended ELM-free phases starts. For the shot with lower D puff, increase of the core radiation is observed during the H-mode termination phase, leading to a faster transition to L-mode (marked as H-L transitions Fig.3c for that shot).

We remark first, that the maximum of the tungsten and nickel cooling rates in the core region is at about 1.4-2keV for coronal distribution (see Fig.4) and second, for the electron temperature lower than 200 eV, the Ni cooling rate in the edge is higher in comparison to W cooling rate and it has a maximum at about 20 eV. In JET ILW, the electron temperature at the separatrix is about 100eV, as can be estimated using a two-point model for the power balance at the separatrix and the L.Frassinetti's pedestal scallings for JET ILW [23]. We point out, that this value is in agreement with our simulations. Since the plasma temperature in the SOL is lower, than that of the separatrix, the cooling rate of Ni is higher than that of W in the SOL (see Fig.4). In addition, it comes out from the simulations that the W density in the SOL is much lower than that of Ni resulting in the very low W radiation in the SOL region of JET ILW ($< 0.14\text{MW}$).

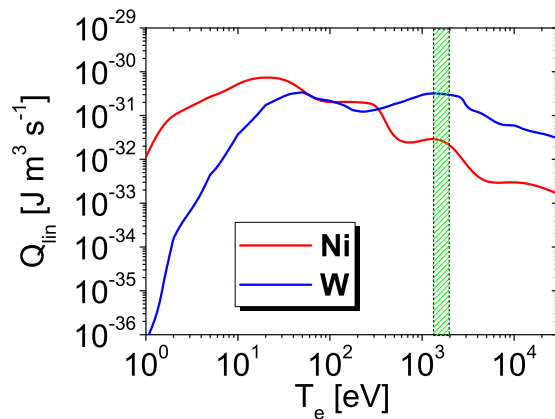


Figure 4. COREDIV cooling rates for nickel (Ni) and tungsten (W) in corona equilibrium.

4. Numerical results

We have studied the influence of the auxiliary heating power and plasma density at the separatrix on the impurity production and transport during the plasma termination phase. Since the deuterium gas fluxes are different, we are assuming that the gas injection controls the separatrix density and the influence of the separatrix density is also analysed. In our simulation, we use four impurities: Be, W self-consistently related by sputtering from divertor targets, and puff of Ne (very small level) in divertor region and puff of Ni. The first source of the nickel particles seen in JET may originate from remote cutting of some Inconel (58%Ni, 21%Cr, 9%Mo) brackets which carried out during the ILW installation [24]. The second source is by ICRF antenna, which is in mid-plane. Although ICRH is the main tool used to prevent W accumulation in the centre of JET plasmas, application of ICRH usually leads to an overall increase of the plasma impurity content, and in particular in JET ILW, tungsten (W) and nickel (Ni) [25, 26]. We remark, that the impact of using antennas with different geometries on core impurity content (W and Ni) was studied in a series of ICRH L-mode pulses where different combinations of antennas were energised [27, 28]. The Ni and W concentration are in the same ballpark for all combinations of antennas used, the ITER-like antenna (ILA) producing slightly less W and radiation when looking at a larger database to comparison with with the other antennas. The source on Ni is the tokamak chamber, and for this reason, in the simulations Ni impurity is represented as a uniform gas puff from the JET wall.

We use in the simulation the same transport model, in which transport coefficients, depend only on confinement time (from scaling law). In particular, the anomalous heat conductivity is given by the expression $\chi_{e,i} = C_{e,i} \frac{a^2}{\tau_E} \times F(r)$, where τ_E is the energy confinement time defined by the ELMy H-mode scaling law (IPB98(y,2)), a is plasma radius and the coefficient ($C_e = C_i$) is adjusted to have agreement between calculated and experimental confinement times. A simple model for the pedestal is

used in COREDIV. The profile function $F(r)$ is defined by the expression $F(r) = [0.25 + 0.75(r/a)^4] \times FSB(r, A)$, where continuous barrier function $FSB(r, A)$ is used to provide the transport barrier in the plasma edge resulting in the barrier width of 5 cm and the height of the pedestal depend on the parameter A (barrier depth reduction factor), which is different between H-mode ($A = 0.15$) and L-mode ($A = 0.5$) to reproduce electron temperature in pedestal.

It should be noted, that $A = 0.15$ is used for all simulation with COREDIV code for H-mode discharges in JET ILW [14, 12].

We point out that the changes of NBI power from its maximum value to about 4 MW are very fast, $\Delta t \sim 0.1$ sec (see Figs. 1 and 2), which is much shorter than the energy confinement time ($\tau_E = 0.32$ sec for $P_{aux} = 28$ MW and $\tau_E = 0.54$ sec for $P_{aux} = 12$ MW). Therefore the plasma parameters are not stationary and they exhibit some kind of inertia (delay). The situation is a bit better in the SOL, where the characteristic times are of the order 10^{-6} - 10^{-5} sec due to very fast plasma (electron) transport along the field lines, at least as regards the main plasma parameters. That means e.g. that the changes to the W source are much faster than the changes to the core plasma parameters.

Since COREDIV is a steady state code, we cannot follow exactly this very fast dynamics of the discharge. Therefore in order to give some insight how the changes of the heating power and deuterium puff level affect the plasma behavior during ramp down phase, we have simulated a sequence of steady state discharges with different input powers and edge densities. Therefore, our results should be treated as a qualitative approach giving indications of the expected trends and not as the precise time dependent simulation of the ramp down evolution. We note also, that the heating power of 12 MW is the lowest power for which the steady state exists. For lower powers, plasma goes to the detachment and cannot be simulated.

Consequently the simulations are performed for different levels of the electron density and auxiliary heating power and compared to experimental parameters at three different times during the ramp-down phase: $t = 13.9$ s; 14.25 s and 14.48 s.

4.1. Influence of the auxiliary heating

For both pulses between time 13.9s and 14.05s, the NBI heating decreases from 26MW to 4MW (see Fig.1 and Fig.2), but ICRH heating is kept constant at the level of 2.6MW and electron density does not change significantly. We would like to explain that the electron density has very strong influence on the discharge dynamics (see [14]). Therefore, in order to analyze only the influence of the auxiliary heating and do not mix it with other effects we have selected shot intervals with similar plasma densities.

In particular, we present the analysis of the influence of the decrease of the auxiliary heating on the tungsten production and Ni and W concentration in the core plasma. The comparison between experimental (at $t = 13.9$ s) and simulated electron density and temperature profiles for different auxiliary heating (all other inputs parameter

unchanged) is presented in Fig. 5. With the decrease of the total auxiliary heating (in experiment only NBI decreases), we observe stronger changes in the central electron temperature in comparison to the pedestal region, where the influence is small.

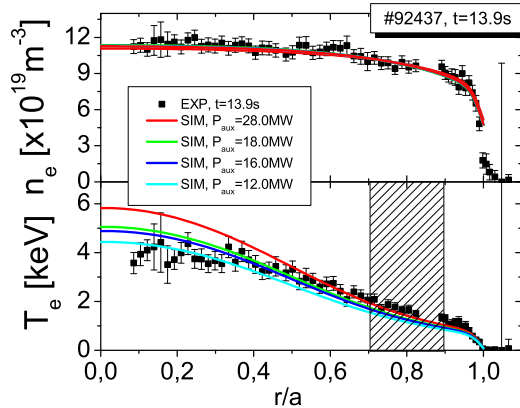


Figure 5. The electron density (top), temperature (bottom) profile from HRTS diagnostic at time $t = 13.9\text{s}$ for # 92437 with different auxiliary heating.

In table 1, we present the main plasma simulated parameters: power to the scrape-off-layer (SOL) (P^{SOL}), power to the plate (P^{PLATE}), electron temperature at the plate in the strike point (T_e^{PLATE}), the total (R^{TOTAL}) and SOL (R^{SOL}) radiations, core line radiation by Ni (R_{Ni}^{LINE}) and by W (R_W^{LINE}), W (C_W) and Ni (C_{Ni}) concentration in the core and W sputtering by W (Γ_{sput}^W) (self-sputtering), by Be (Γ_{sput}^{Be}) and by Ni (Γ_{sput}^{Ni}). The Be core concentration in the simulation is about 0.7%. We note also, that the heating power of 12 MW is the lowest power for which the steady state exists. For lower powers, plasma goes to the detachment and cannot be simulated. We observe, that with decrease of the heating power, the temperature in the core and also power to the SOL decrease, and since the radiation in the SOL does not change, the power and temperature at the plate decrease. In this situation, the decrease of the W production is observed. We remark that for temperature on the plate, $T_e^{PLATE} < 5\text{eV}$ the main source of W is sputtering mainly by Ni. With the heating power decrease and related decrease of the plate temperature, opposite behaviour of W and Ni was observed: W concentration decreases from 2.67×10^{-5} to 0.06×10^{-5} , which could be explained by lower production from the plate (see Γ_{sput}^W , Γ_{sput}^{Be} , Γ_{sput}^{Ni} in Table 1), but core Ni concentration increases by 20% and the core Ni radiation is enhanced by 30%. This is could be explained qualitatively by the Ni cooling rate (see Fig. 4). For the $P_{aux} = 12\text{MW}$, Ni is the dominant radiator in core and SOL region. Good correlation between experiment and simulation at $t = 13.9\text{s}$ is observed for the impurity concentration C_W (0.5×10^{-5}) and C_{Ni} (1.1×10^{-4}).

The radial profile of the total, bremsstrahlung, W and Ni radiation in the core for this time ($t = 13.9\text{s}$) from simulation is presented in Fig. 6. Nickel (green line) show two maxima of the radiation: one near the separatrix and the second for $r/a \sim 0.75$. We remark, that maximum of the radiation by Ni and W is at the same normalized

Table 1. Main plasma parameters with different auxiliary heating

Parameters	$P_{aux}=28\text{MW}$	$P_{aux}=18\text{MW}$	$P_{aux}=16\text{MW}$	$P_{aux}=12\text{MW}$
P^{SOL} [MW]	19.7	14.3	12.9	10
P^{PLATE} [MW]	15.2	9.7	8.3	5.5
T_e^{PLATE} [eV]	8.3	6.7	5.1	3.9
R^{TOTAL} [MW]	13.1	8.96	8.2	7.6
R^{SOL} [MW]	4.5	4.6	4.6	4.5
R_{Ni}^{LINE} [MW]	1.9	2.3	2.35	2.46
R_W^{LINE} [MW]	6.0	1.1	0.6	0.2
C_W [$\times 10^{-5}$]	2.67	0.5	0.2	0.06
C_{Ni} [$\times 10^{-4}$]	1.03	1.17	1.22	1.23
Γ_{sput}^W [$\times 10^{19}$ 1/s]	1.32	0.1	0.025	0.025
Γ_{sput}^{Be} [$\times 10^{19}$ 1/s]	1.9	0.7	0.4	0.028
Γ_{sput}^{Ni} [$\times 10^{19}$ 1/s]	1.2	0.5	0.36	0.1

radius ($1.4\text{keV} < T_e < 2\text{keV}$). The radiation around X – point is emitted by Ne and Ni, which correlates well with the tomographic reconstruction (see Fig. 7).

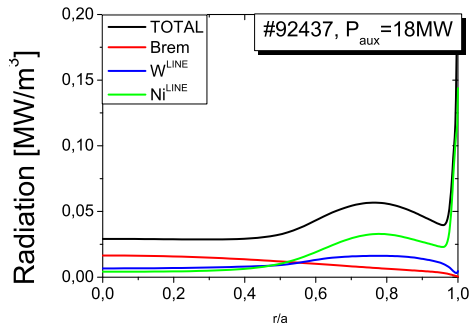


Figure 6. Profile of the core radiation at $t = 13.9\text{s}$.

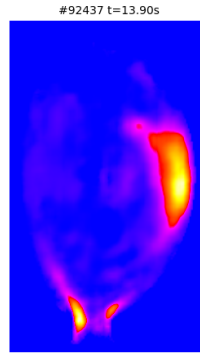


Figure 7. Tomographic reconstruction of the radiated power density for shot # 92347 at time $t = 13.9\text{s}$.

Regarding the simulation of the second time slice ($t = 14.25\text{s}$) with lower auxiliary power (9 MW), the reconstructed radiation profile is shown in Fig. 8 and the tomographic reconstruction in Fig.9.

Decrease of the heating power affects temperature in the core resulting in the inward shift of the maximum of the radiation from $r/a = 0.75$ to $r/a = 0.5$. The radiation is also more uniform in the core.

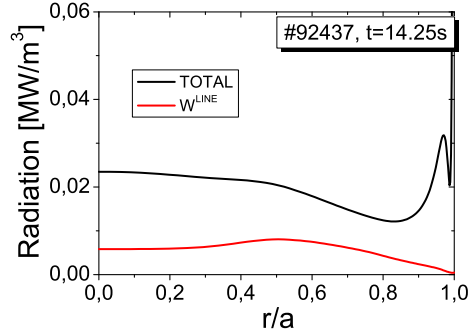


Figure 8. Profile of the core radiation at $t=14.25s$.

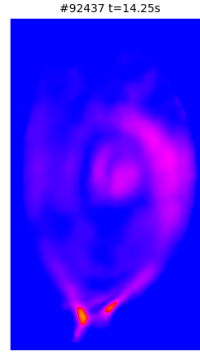


Figure 9. Tomographic reconstruction of the radiated power density for shot # 92347 at time $t = 14.25s$.

4.2. Influence of the separatrix density

In the simulation for the time point $t = 14.48s$ with auxiliary heating $P_{aux}=7MW$ we use a different peaking factor for density profile, to take into account the effect of different confinement $H_{98} = 0.58$ (0.75 for $t=14.25s$). The influence of the separatrix density on the plasma electron density and temperature, which might be connected with different deuterium puff in the experiment, is simulated and shown in Fig. 10. With the decrease

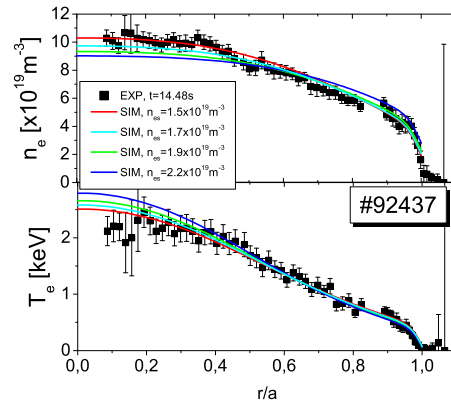


Figure 10. Experimental (HRTS) and reconstructed T_e and n_e profiles at $t = 14.48s$ with difference density on the separatrix (n_{es}).

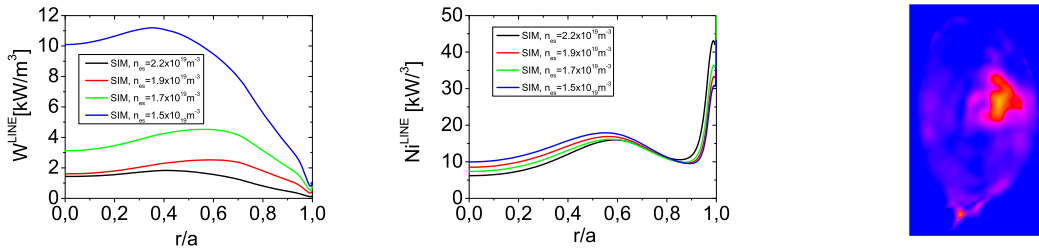
of the electron separatrix density, keeping the same volume average density, we observe the increase of the density in the centre (comparison between red and blue line) and the related decrease of the central temperature. The main plasma parameters versus different separatrix density are presented in Table 2. With the decrease of the separatrix density (lower fueling), increase of the temperature on the plate is observed. As a

Table 2. Main plasma parameters with different separatrix density

$n_{es} [\times 10^{19} m^{-3}]$	2.2(0.31 n_e)	1.9	1.7	1.5(0.23 n_e)
T_e^{PLATE} [eV]	5.32	6.8	7.7	10.6
R_{TOTAL} [MW]	4.43	3.9	3.8	4.0
R_{SOL} [MW]	2.27	1.9	41.7	1.45
$C_W [\times 10^{-5}]$	0.8	1.2	2.2	4.5
R_W^{LINE} [MW]	0.13	0.18	0.31	0.7
$C_{Ni} [\times 10^{-4}]$	1.	0.98	1	1.05
R_{Ni}^{LINE} [MW]	1.51	1.44	1.45	1.49

results W production increases which could lead to an increase of the W concentration in the discharge. This is agreement with SXR measurements (see Fig.3a). We note, that decrease of the separatrix density by 25% resulted in a 5 times increase of the W radiation and W concentration in core. The change of the separatrix density in this case hardly influences the Ni concentration, which could be related to the interplay between friction and thermal forces being affected by the changes to the separatrix density.

The influence of the separatrix density changes on the profiles of the radiated power (simulated and experimental) at $t = 14.48s$ is shown in Fig. 11. The maximum of the W and Ni radiation is seen to move towards the centre. The dominant radiation in the core region is by nickel.

**Figure 11.** Tomographic reconstruction of the radiated power density for shot #92347 at time $t = 14.48s$.

5. Summary

The main conclusion from the preliminary simulations is the observation that for the same average electron density, the decrease of the auxiliary power leads to the reduction of the W production (sputtering) and to the reduction of the core temperature leading to the shift of the maximum of the radiation towards the plasma centre. In the considered shot, the decrease of the separatrix density leads to an increase of the plasma temperature at the divertor plate leading to increased W production and consequently to

larger W concentration and radiation in the core. When the central electron temperature approaches the 2keV level, corresponding to the maximum of the W and Ni cooling rate, enhanced radiation in the plasma center occurs.

It comes out from the simulations that the main contributor to W sputtering is nickel. For this reason the control of the Ni in ramp-down is more important.

5.1. Acknowledgments

This work has been carried out within the framework of the EUROfusion Consortium and has received funding from the Euratom research and training programme 2014-2018 and 2019-2020 under grant agreement No 633053. The views and opinions expressed herein do not necessarily reflect those of the European Commission.

This scientific work was partly supported by the Polish Ministry of Science and Higher Education within the framework of the scientific financial resources in the year 2020 allocated for the realization of the international co-financed project No 5118/H2020/EURATOM/2020/2.

6. References

- [1] Wesson J., Tokamaks, volumen 1. Clarendon Press, Oxford, England, (2004)
- [2] de Vries P.C., et al., Nucl. Fusion 51 (2011)
- [3] Bizaro J., et al., Plasma Phys. Control. Fusion 58 (2016)
- [4] Joffrin E., et al., in Proc. 26th IAEA Fusion Energy Conference, Kyoto, Japan (2016)
- [5] Lehnen M., et al., Nucl. Fusion 53 (2013)
- [6] Hogewey G.M.D., et al., Nucl. Fusion 55 (2015)
- [7] F.Koechl, et al., Nucl. Fusion, 57, 086023 (2017)
- [8] Neu R., et al, Physics of Plasma, 20, 056111 (2013)
- [9] Dux R., et al., Nuclear Materials and Energy 12 (2017)
- [10] de la Luna E., et al., Nucl. Fusion 56 (2016)
- [11] de la Luna E., et al., Impact of ELM control in JET experiments on H-mode terminations with/without current ramp-down and implications for ITER //Proc. IAEA conference(2018)
- [12] Ivanova-Stanik I., et al., Contrib. Plasma Phys. 54, No. 4-6 (2014)
- [13] Telesca G., et al., J. Nucl. Mater., 463 (2015)
- [14] Zagórski R., et al., J. Nucl. Mater., 463 (2015)
- [15] Telesca G., et al., Nucl. Fusion 57 (2017)
- [16] Zagórski R., et al., Nucl. Fusion 53 (2013)
- [17] Yamamura Y., et al., Report of the Institute of Plasma Physics Nagoya, IPPJ-AM-26 (1983)
- [18] Kallenbach A., et al., Plasma Phys. Control. Fusion 60 (2018)
- [19] Mlynar J., et al., Proc. of the 28th Symposium on Fusion Technology SOFT, San Sebastian, Spain (2014)
- [20] Putterich T., et al., Plasma Phys. Control. Fusion 55 (2013)
- [21] Krawczyk N., et al., Review of Scientific Instruments in 22nd Topical Conference Proceedings on High-Temperature Plasma Diagnostics (HTPD) (2018)
- [22] Lawson K.D., et al., JINST 4 P04013 (2009)
- [23] Frassinetti L., et al., Nucl. Fusion in pres (<https://doi.org/10.1088/1741-4326/abb79e>) (2020)
- [24] Matthews G.F., et al., J. Nucl. Mater. 438 (2013)
- [25] Czarnecka A., et al., Plasma Phys. Control. Fusion 53 (2011)

- [26] Czarnecka A., et al., Proce.of 20th Topical Conference on Radio Frequency Power in Plasmas, Sorrento, Italy,June (2013)
- [27] Bobkov A., et al., J. Nucl. Mater. 438 (2013)
- [28] Jacquet P., et al., EPJ Web of Conferences 157 (2017)